JOURNAL OF MATERIALS SCIENCE 32 (1997) 6201–6205

Cellular growth and dislocation structures in laser-nitrided titanium

A. B. KLOOSTERMAN, J. TH. M. DE HOSSON*
Department of Applied Physics, Materials Science Centre, University of Groningen, Nijenborgh 4, 9747 AG Groningen, The Netherlands

Transmission electron microscopic observations were made of different dislocation structures in laser-nitrided titanium. Equidistant edge dislocations in the bulk and periodic surface structures exhibit a periodicity within the same order of magnitude. An analysis is presented in which both periodic phenomena are explained by cellular growth.

1. Introduction

Titanium possesses several excellent properties like a good corrosion resistance and high strength to weight ratio. Its light weight and ability to withstand extreme temperatures make titanium suitable for aerospace applications. However, a disadvantage of titanium is its high friction and poor wear resistance. This problem can be tackled by applying a protective coating, for instance by nitriding the surface which results in a hard ceramic surface layer and as a consequence enhances both wear and friction properties. Nitriding with techniques like chemical vapour deposition (CVD) and physical vapour deposition (PVD) produces a limited surface layer of a few micrometres [1]. In contrast, laser nitriding may result in a modified layer of several hundreds of micrometres [2–8]. This high-temperature treatment results in various microstructural features.

In this study, titanium samples were laser nitrided with the use of a 1.5 kW CO_2 laser at different laser-scan velocities. The modified layer contained different microstructures with their own specific hardness. At the top of this layer, a thin (1–3 μm), flat and highly $\{1\,0\,0\}$ textured TiN layer was observed. Perpendicular to this, TiN dendrites were present. The top layer contained periodic structures which were observed both by scanning and transmission electron microscopy, although being different in appearance. TEM observations showed fuzzy lines, whereas SEM observations demonstrated an undulated surface. The periodicity of the dislocation structures was of the same order of magnitude as the surface structure observed with the SEM. With increasing laser-scan velocity, the periodicity decreased, where finally a transition to dendritic growth took place.

During solidification after laser processing, the orientation of the top layer is determined by the crystallographic preferred direction for heat transport. By considering the phonon spectrum it can be seen that the growth direction corresponds with the direction of strongest phonon interactions. Further, cracks were present in the modified layer, caused by high thermal stresses which exceeded the critical stress for fracture. These cracks tended to follow certain preferred crystallographic directions.

2. Experimental procedure

Commercially pure (grade 2) titanium sheets with a thickness of 5 mm and a diameter of 40 mm were laser treated. This was done with the use of a 1.5 kW Spectra Physics CO_2 laser operating in a TEM_{00} mode, which resulted in a Gaussian intensity distribution. Before processing, the samples were sand blasted to increase the absorption of the laser beam. The applied laser power was 1200 W and the scan velocity was in the range of 25–200 mm s^{-1}. The beam diameter amounted to 0.55 mm. The nitrogen flow was supplied by a nozzle system consisting of three nozzles with an axial and two side flows under an angle of 45°.

Subsequently, cross-sectional and top-view TEM specimens were made. Samples of the top layer were ground from the bulk side, dimpled and finally ion milled. When the first hole arose, the sample was ion milled from above for about 45 min. Cross-sectional TEM specimens were made by taking a slice, grinding both sides to a thickness of around 10 μm and finally ion milling from one side under alternating positive and negative angle until some material was removed from the top layer.

The surface morphology was studied with the use of a Philips FEG XL30 scanning electron microscope. Further a Jeol-200 CX and a Jeol-4000EX-II transmission electron microscope, operating at 200 and 400 kV, respectively, were used to study the dislocation structures and to determine the different phases. The advantage of the latter microscope was that, al-

* Author to whom all correspondence should be addressed.

0022–2461

though the sample contained differences in thickness due to different thinning rates for titanium and TiN, the electrons penetrate the sample more easily.

3. Results

On top of the laser track, a flat, thin TiN layer was present if the laser power density (LPD) was high enough to melt TiN. TiN dendrites were oriented perpendicular to this TiN layer, whereas deeper in the melt the dendrites became randomly oriented. The microstructure in between the dendrites consisted of a very fine needle-like structure (Fig. 1), which was also present below the dendritic region [2]. Locally, there existed a preferred orientation between the needles in two directions, often varying between 60° and 90°. Because laser treatment of titanium in an argon atmosphere did not result in this needle-like structure, this must be influenced by the interstitial presence of nitrogen atoms. The phase was determined with the use of the TEM. The needles appeared to have an hcp phase in accordance with the phase diagram. The needles were likely formed by a martensitic phase transformation from the β-phase. Fig. 2 shows two or three needles almost in the same diffraction condition. Note that for this case, the angular orientation of the needles with respect to each other, amounts to 60°.

At a micrometre scale, the surface morphology can be described by large, flat grains and ripples. The grains tended to grow perpendicular to the solidification front which was indicated by ripple contours [2, 3]. Around the middle of the tracks the grains were elongated for low velocities, where at increasing velocity their length decreased in order to maintain growth perpendicular to the front. The solidification front was V-shaped which became more ragged for increasing scan velocity.

X-ray measurements showed the surface to exhibit strong $\{0\,0\,1\}$ texture. TEM research established elongated grains positioned around the $\{0\,0\,1\}$ orientation with respect to the surface and growing in a $\langle 1\,0\,0\rangle$ direction. Neighbouring grains in the middle of the track were tilted in random directions over a few degrees.

TiN was supposed to have the same slip system as NaCl. Edge dislocations were expected to be situated in the $\{1\,1\,0\}$ plane and screw dislocations in the $\{1\,0\,0\}$ plane due to their different mobilities in the different planes [9]. Nevertheless, at high temperatures, deviations could occur, caused by a decrease of the ionic nature of bonding. In the TiN top layer, screw dislocations were found with Burgers vector $\pm\frac{1}{2}[1\,\bar{1}\,0]$. Fig. 3 shows a network of screw dislocations. Locally, these consisted of only one type but there were also places where screw dislocations with both $\boldsymbol{b} = \pm\frac{1}{2}[1\,\bar{1}\,0]$ and $\boldsymbol{b} = \pm\frac{1}{2}[1\,1\,0]$ were present.

Besides screw dislocations, edge type dislocation structures were also found, which can be seen in Fig. 3. We expected to find $\boldsymbol{b} = +\frac{1}{2}[1\,1\,0]$, which is the shortest translational invariant lattice vector, but we found $\boldsymbol{b} = [0\,1\,0]$ which implies the dislocation being sessile. In contrast to the screw dislocations, the edge dislocation lines were quite fuzzy. It seemed like there were a number of dislocation lines, heavily jogged and kinked, in a very narrow band. In the middle of the laser track, all edge dislocation lines were parallel to the laser scan direction and/or solidification direction

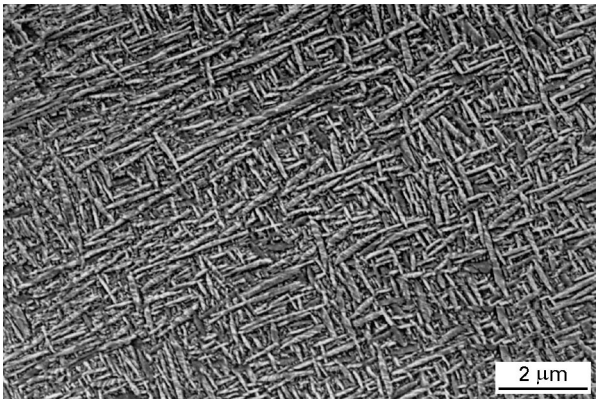

Figure 1 Scanning electron micrograph showing needle-like structure.

Figure 2 Bright-field transmission electron micrograph of two or three needles being almost in the same diffraction condition.

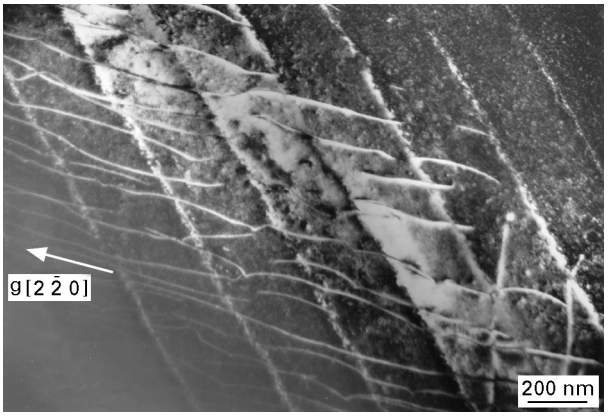

Figure 3 Dark-field, weak-beam transmission electron micrograph showing dislocation structures of TiN at a laser scan velocity of 50 mm s^{-1}. The fuzzzy equidistant lines represent the edge dislocation lines, which run along the [2 0 0] direction. The lines under 45° with respect to the equidistant structure represent the screw dislocations.

and formed a regular equidistant structure. The spacing was found to be dependent on the laser scan velocity. For laser scan velocities of 50 and 100 mm s^{-1} we found a period of 265 and 210 nm, respectively. It seemed to be almost impossible to obtain periodicities for higher scan velocities because of thermal stresses which generate problems during sample preparation. Considering the Kikuchi patterns, only one band in between two edge dislocations could be in the exact diffraction condition. This means that low-angle grain boundaries were formed with an angular tilt between two bands of 0.2°–0.4°.

Parallel to TEM observations of equidistant edge-type dislocations, the surface layer of TiN was studied with SEM, which established equidistant surface structures with periods of the same order of magnitude (Fig. 4). For scan velocities between 50 and 100 mm s^{-1}, almost the complete surface of the laser track was covered with the equidistant structure, whereas outside this velocity range (above and below) the percentage was strongly reduced. For scan velocities of 150 mm s^{-1} and higher, dendritic structures also emerged at the surface, as depicted in Fig. 5. The periodicity for a certain scan velocity was determined by averaging over at least six different positions, where at each position the average was taken over at least ten periods. To enable an accurate comparison between the SEM and TEM observations, only periodic structures in the middle of the laser track were considered. Further, only stable arrays of cells without tip splitting, overgrowth and a little side branching, were taken into account. Table I shows the periodicities as a function of the laser scan velocity. The relation between the periodicity and the solidification velocity will be discussed later.

With SEM, cross-sections were studied to see if there was a step-wise surface structure implying slip or an undulated surface indicating cellular growth. This was rather difficult because the height differences were about 10–30 nm in size, which required accurate preparation of cross-sections. Both surface structures were observed, where the undulated surface can be split up into different appearances (Fig. 6). This can be explained by an excess or a shortage of material during solidification, resulting in elevation or lowering of the surface, respectively. The undulated surface was more regular than the stepwise surface. Because of this and a probably different phenomenon, namely slip, the stepwise structure was not incorporated in the average value of the periodicity.

At the surface, cracks were observed, which most of the time traverse the equidistant structure perpendicularly (Fig. 7). This gives an indication for the strongest bonds, Ti–Ti or Ti–N. For {1 0 0} cleavage planes, there is a higher proportion of broken metal to non-metal bonds. If we only consider the nearest neighbour interaction, this means that the Ti–Ti bond is stronger than the Ti–N bond. Nevertheless, {1 1 0} cleavage planes were also observed but less frequently.

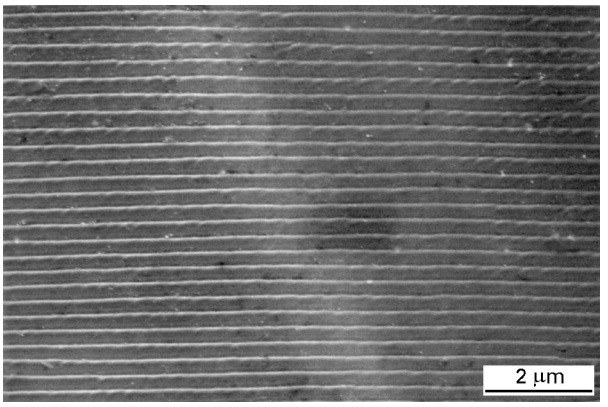

Figure 4 Scanning electron micrograph showing periodic surface structure.

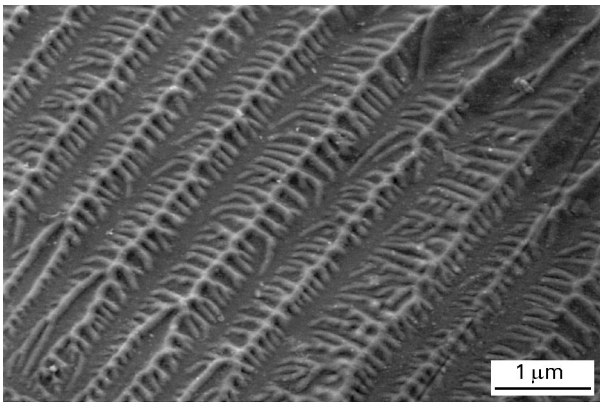

Figure 5 Scanning electron micrograph showing dendritic structures at the surface (scan velocity 200 mm s^{-1}).

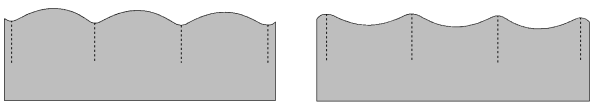

Figure 6 Schematic representation of the two different periodic surface structures which are observed in cross-section. (– – –) The probable position of the edge dislocations.

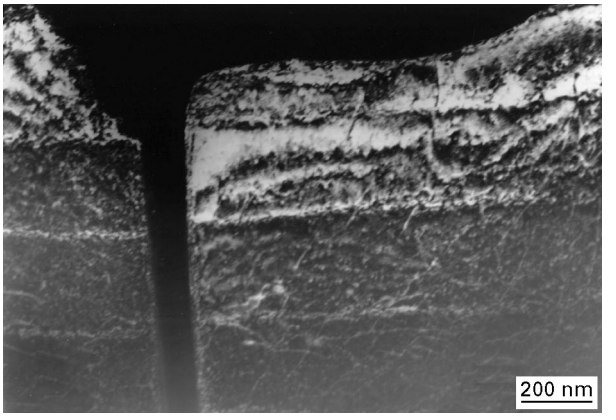

Figure 7 Dark-field, weak-beam transmission electron micrograph showing a crack propagating perpendicular to the equidistant structure.

4. Discussion

The type of screw dislocation in the TiN layer corresponds with the expectation for the NaCl type of crystal structures, in contrast to the type of edge dislocation found. At first sight, the presence of edge dislocations with Burgers vector [0 1 0] could be explained by the clustering and recombination of two edge dislocations with Burgers vector $\frac{1}{2}[1\,1\,0]$ and $\pm\frac{1}{2}[\bar{1}\,1\,0]$. However, separate Burgers vectors were never observed, which does not make this assumption realistic.

The periodic edge dislocations arise as fuzzy lines, which is different from the way the screw dislocations occur. Probably this can be explained by the presence of segments of dislocation lines, which are heavily jogged and kinked. Initially we supposed the dislocation structures to be regularly spaced to minimize their energy. As a consequence, the periodicity was possibly imposed by the thermal stresses after laser processing. However, by considering the SEM observations, the explanation turned out to be different.

Because the periods are of the same order of magnitude, the question remains how to connect the periodic edge dislocations in the TiN layer with the periodic surface structures. The SEM observations indicate cellular growth, which makes it plausible to connect the cellular interface with the dislocation lines. However, why does the interface behave like being an edge-type dislocation? Therefore, the solidification process conditions have to be taken into account. Locally, the growth of the cells is quite stable without overgrowth and tip splitting. Further, the growth orientation, which is restricted by the heat transport, is nearly the same for two adjacent cells. If the large amplitude cells are a little tilted with respect to each other while joining together, there will be some misfit at the interface. In the case of a small tilt around an axis parallel to the dislocation lines, the misfit can be described in terms of edge dislocations. If we take into account the growth direction [0 1 0] towards each other, the final interface can be described by edge dislocations with Burgers vector [0 1 0], which corresponds with the experimental observations.

In order to determine the preferred growth direction, we have to consider the heat transport in the various crystallographic directions. Cellular solidification takes place in the direction of the temperature gradient, which is perpendicular to the solidification front, and is controlled by the thermal conductivity. The latter bears properties of a second-rank tensor. From electronic band-structure calculations [10] it can be concluded that TiN, in comparison with pure titanium, exhibits a shift of the 3d bands downwards through the Fermi energy level, where 4s electrons of titanium are transferred to 2p bands of nitrogen. As a consequence, the 3d orbitals of titanium in TiN become hybridized to a considerable degree with the 2p wave functions of nitrogen. This results in a bonding orbital filled by 2p and 3d electrons. At the Fermi level, TiN points to a metallic behaviour with electron conduction, whereas titanium shows partial hole conduction due to the strong negative curvature of 3d energy bands (hole pockets) near the Fermi level. Indeed, experimentally, TiN is found to be a metallic conductor. At first sight, the thermal conductivity in TiN is due to electrons as heat carriers. The dominant scattering mechanisms would be defects at lower temperatures and phonons at higher temperatures. In a molecular orbital description, which is simpler than a full self-consistent electronic band structure calculation [10], it is easy to see that the π-bonding, that is the d–p hybridization, between the 3d orbitals of titanium and 2p orbitals of nitrogen leads to an electrical and thermal conductivity along the cubic $\langle 1\,0\,0\rangle$ directions. It should be emphasized that, although TiN shows metallic behaviour, it does not necessarily mean that the temperature dependence of the thermal conductivity is pure metallic. Actually, it was pointed out that the thermal conductivity of TiN and TiC exhibit an increase with temperature [11, 12], in contrast to pure metals where the thermal conductivity is almost independent of temperature. It was proposed [13] that the thermal conductivity is dominated by the electrons as heat carriers and not by the phonons. The former contribution increases as a function of temperature due to the numerous defects present in TiN and TiC, whereas the phonon scattering by defects reduces the lattice conductivity.

During solidification of an alloy, different growth morphologies may appear, such as planar front, cellular, dendritic and eutectic structures. The solidification conditions determine which of these structures is stable, where the cellular and dendritic structures can be characterized by tip radius, primary and secondary arm spacings. In fact, the solidification of the microstructure is determined by physical phenomena like solute and thermal diffusion, interfacial free energy, where in the case of laser processing convection also may play an important role. In general, the relation between the processing parameters and the characteristic microstructural length is given by

$$\lambda \propto G^{-a}V^{-b} \tag{1}$$

where λ is the cellular spacing, G the temperature gradient at the solidification front and V the velocity of the solidification front [14]. This relation turned out to be valid for dendrites, whereas for cells a rather complicated relationship is required due to the different velocity regime in which this structure appears [14]. Despite this, it turned out that many experimental results can be approximated by the above formula. Recently, Hunt and Shu-Zu Lu [15] presented a numerical solution for cellular growth close to the well-known relation

$$\lambda^2 v_s = \text{constant} \tag{2}$$

However, this was a rough guide over a large velocity range. For a limited range, deviations could occur, particularly for low-velocity cells. Note that for the numerical solution, the cell spacing is independent of the temperature gradient. Nevertheless, many other solutions have been found in the past, where a varies between 0.15 and 0.56 and b between 0.25 and 0.6 [13, 16].

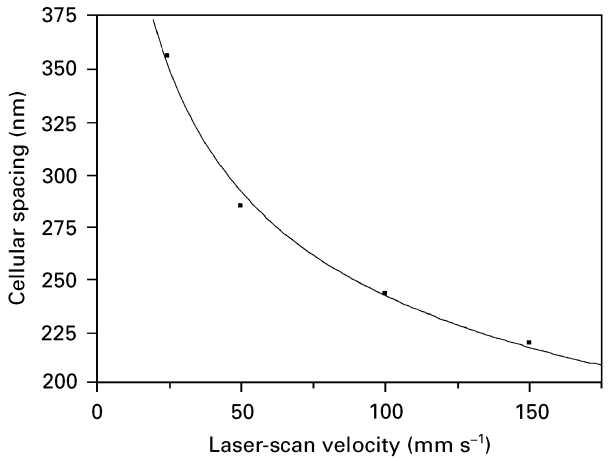

Figure 8 Cellular spacing as a function of the laser-scan velocity. (——) $\lambda \propto v_l^{-0.27}$.

The experimental results exhibited cellular growth for scan velocities in the range between 25 and 150 mm s^{-1}, where the cellular spacing was found to decrease with increasing scan velocity. Above 150 mm s^{-1}, dendritic growth structures were also present, whereas the primary arm spacings were not stable over a large range. Although the average value of the cellular spacing was taken, it must be mentioned that there exists a certain range of values for every solidification velocity. Fig. 8 shows the experimentally found cellular spacing as a function of the laser-scan velocity. Calculations of the square root of temperature gradient at the solidification front indicate that these are almost the same for the velocity regime considered. The calculations were done by using an analytical model which incorporated a Gaussian energy distribution of the laser beam [17]. Further phase transformations and temperature dependence of physical properties were neglected. If we assume the solution to be independent of the temperature gradient the best fit is given by $\lambda \propto v_l^{-0.27}$.

5. Conclusion

With respect to the TiN top layer, the equidistant dislocation structure was induced by cellular growth. Further, cellular growth caused an undulated surface structure. A small misorientation of adjacent cells resulted in low-angle grain boundaries, where at the cellular interface, edge dislocations were formed with a Burgers vector [0 1 0]. The relation between the laser-scan velocity and the cellular spacing was found to be $\lambda \propto v_l^{-0.27}$.

Acknowledgement

Special thanks are due to Marco Workel for his contributions. This work is part of the research programme of IOP-Metalen, The Hague, The Netherlands, and of the Foundation for Fundamental Research on Matter (FOM-Utrecht) and has been made possible by financial support from the Netherlands Organization for Research (NWO-The Hague)

References

1. S. CHATTERJEE, T. S. SUDARSHAN and S. CHANDRASHEKHAR, *J. Mater. Sci.* **27** (1992) 1989.
2. A. B. KLOOSTERMAN and J. TH. M. DE HOSSON, *Scripta Metall. Mater.* **33** (1995) 567.
3. S. MRIDHA and T. N. BAKER, *Mater. Sci. Eng.* **A188** (1994) 229.
4. B. L. MORDIKE, in "Laser Surface Treatment of Metals", edited by C. W. Draper and P. Mazzoldi (Kluwer, Dordrecht, 1986) p. 389.
5. T. BELL, H. W. BERGMANN, J. LANAGAN, P. H. MORTON and A. M. STAINES, *Surface Eng.* **2**(2) (1986) 133.
6. P. H. MORTON, T. BELL, A. WEISHEIT, J. KROLL, B. L. MORDIKE and K. SAGOO, *Surface Modif. Technol.* **V** (1992) 553.
7. M. IGNATIEV, E. KOVALEV, I. MELEKHIN, I. YU. SMUROV and S. STURLESE, *Wear* **166** (1993) 233.
8. J. FOLKES, D. R. F. WEST and W. M. STEEN, in "Laser Surface Treatment of Metals", edited by C. W. Draper and P. Mazzoldi (Kluwer, Dordrecht, 1986) p. 451.
9. L. HULTMAN, M. SHINN, P. B. MIRKARIMA and S. A. BARNETT, *J. Crystal Growth* **135** (1994) 309.
10. E. VOGELZANG, J. SJOLLEMA, H. J. BOER and J. TH. M. De HOSSON, *J. Appl. Phys.* **61** (1987) 4606.
11. R. E. TAYLOR, *J. Am. Ceram. Soc.* **44** (1961) 525.
12. W. S. WILLIAMS, *ibid.* **49** (1966) 156.
13. D. G. McCARTNEY and J. D. HUNT, *Acta Metall.* **29** (1981) 1851.
14. W. KURZ and D. J. FISHER, *ibid.* **29** (1981) 11.
15. J. D. HUNT and SHU-ZU LU, *Metall. Mater. Trans. A* **27** (1996) 611.
16. SHU-ZU LU and J. D. HUNT, *J. Crystal Growth* **123** (1992) 17.
17. D. ROSENTHAL, *Trans.* ASME **68** (1946) 349.

Received 20 March
and accepted 29 May 1997